Coastal Dynamics 2017
Paper No. 145

WAVE HEIGHT AND BATHYMETRIC CONTROLS ON SURFZONE CURRENT VELOCITY AND DISPERSION ACROSS AN EMBAYED BEACH

R. Jak McCarroll[1], Robert W. Brander[2] and Tim Scott[1]

Abstract

Forcing relationships between wave height, 3D-bathymetry and surfzone currents were investigated across an embayed beach with an alongshore energy gradient. Controls on velocity variability and dispersion over 3D bathymetry in particular are poorly understood. Breaking wave height (H_b) was numerically modelled and alongshore depth standard deviation (σ_z) quantified three-dimensionality. Lagrangian drifters observed embayment-wide currents over a 3 h period, providing mean velocity (U), velocity standard deviation (σ_U) and dispersion (D). Positive linear relationships were found between H_b and both U ($R^2 = 0.26, p = 0.002$) and σ_U ($R^2 = 0.50, p < 0.001$). While σ_z was correlated only with U ($R^2 = 0.21, p = 0.01$), and D was uncorrelated with H_b and σ_z. This study contributes new methods for understanding surfzone forcing relationships and is the first attempt to examine spatially-variable surfzone dispersion.

Key words: Embayed intermediate beach, Bondi Beach, rip currents, Lagrangian drifters and surfzone eddies.

1. Introduction

Intermediate embayed beaches are convenient natural laboratories for investigating forcing controls on surfzone currents as they often exhibit an alongshore wave height gradient and equilibrium parabolic planform (Hsu et al., 2010), with increasing curvature toward the protected end of the beach. The higher energy end of the beach typically has higher waves, a wider surfzone and higher energy beach-state morphology (Wright and Short, 1984; Short 1999).

For transitional embayed beaches (~1 km in length; Castelle and Coco, 2012), a steep alongshore energy gradient can result in rapid changes in morphology over short distances (McCarroll et al., 2016) and several types of surfzone currents can be expected to occur across the beach. Channelised rip cells (Castelle et al., 2016) are a common feature, forced by greater breaking over shallow bars relative to deeper rip channels (Bowen, 1969). Rip currents are also common occurrence at the boundary headlands (Castelle and Coco, 2013), though are not the focus here. Alongshore currents are expected to be minimal in an equilibrium bay due to refraction toward shore-normal, with the exception of the alongshore components of rip cells (Silva et al., 2010; Castelle and Coco, 2013).

Channelised rip currents are known to increase in mean flow velocity as: (i) wave energy increases; (ii) water levels decrease; and (iii) bathymetric three-dimensionality increases (MacMahan et al., 2006; Castelle et al., 2016). These forcing controls are typically demonstrated for a single point in an isolated rip channel, however, it is of interest to know how generalisable these relationships are, to all regions within the surfzone, over various morphologies, under variable forcing. One effort to generalise the relationship between mean current and bathymetric three-dimensionality (McCarroll et al., 2014) found a clear correlation along an embayed beach, albeit over a simple morphology with minimal alongshore wave height variation.

In addition to mean flows forced by 3D-morphology, surfzone currents vary at low frequencies

[1]Coastal Processes Research Group, Plymouth University. jak.mccarroll@plymouth.ac.uk
[2]School of Biological, Earth and Environmental Sciences, UNSW Australia.

(O[10 min]) due to stochastic vortical forcing by a directionally spread wave field (Peregrine, 1999) produced by transient alongshore variations in wave height and dissipation. This manifests on planar morphology as transient surfzone eddies (e.g. Spydell et al., 2007; Feddersen, 2014) and flash rips exiting the surfzone (Johnson and Pattiaratchi, 2006; Suanda and Feddersen, 2015). On 3D-morphology, variable forcing can result in intermittent pulsations of rip channel flows, switching between recirculation within the surfzone and exit trajectories beyond the surfzone (Reniers et al., 2009; MacMahan et al., 2010; Castelle et al., 2014).

Exceedingly few field studies have examined low-frequency flow variability over three-dimensional morphology within the surfzone (MacMahan et al., 2004; Brown et al., 2009), consequently, this area is poorly understood (Castelle et al., 2016). Rates of dispersion (diffusivity) on 3D-morphology were investigated by Brown et al., (2009), comparing diffusivity on bar-rip morphology to a similar study on planar morphology (Spydell et al., 2007) and while some evidence suggested that diffusivity increased with wave height and period, no conclusive relationships were established between wave conditions, bathymetry and diffusivity. Observations of low-frequency flow variability on bar-rip morphology (MacMahan et al., 2004) demonstrated a significant correlation between wave height and low-frequency velocity variability, and that velocity variability was approximately constant over adjacent bars and rip channels, additionally it hypothesised that rip-cells respond to low-frequency changes in forcing by oscillating in the cross-shore. The field observations of MacMahan et al. (2004) were expanded upon with numerical modelling (Reniers et al., 2007), suggesting that velocity variability increases with bathymetric three-dimensionality and lower water levels. A laboratory study of a moveable beach over a full downstate transition (Castelle et al., 2010) suggested that high (low) bathymetric three-dimensionality was associated with strong (weak) velocity variability and weak (strong) directional variability. Each of these relationships is preliminary, requiring further observational testing in different conditions, or has been limited to modelling results.

This study aims to present a method and a preliminary case study for generalised testing of the above hypothesised scaling relationships, some of which are well established for specific scenarios, others of which are largely undetermined. An embayed beach with an alongshore wave height gradient is used as the laboratory, flow behaviour is measured with Lagrangian drifters and breaking wave heights are determined using a wave transformation model. The relationships to be tested include: (i) breaking wave height as a forcing control on bathymetric three-dimensionality, mean current velocity, variable velocity and rates of dispersion; and (ii) bathymetric three-dimensionality as a forcing control on mean current velocity, variable velocity and rates of dispersion.

2. Field Site

Field observations were conducted at Bondi Beach, Sydney, Australia (Fig 1). Mean offshore significant wave height (H_s) is 1.6 m, with a peak period (T_p) of 10 s (Short and Trenaman, 1992). The beach is 850 m long and deeply embayed with a strong alongshore energy gradient. The SW end is energetic with a wide surfzone, fully exposed to the dominant SSE swell, while the NE corner is a low-energy zone protected by a headland and offshore sub-aqueous ridge. The beach state at the SW end is high-energy intermediate, often with complex multiple-bars and rip channels (McCarroll et al., 2016), grading to a modal low-tide-terrace to the NE. Tides are micro-tidal (<2 m spring range), sediment is medium grained quartz sand.

3. Methods

3.1. Field observations

Over the period July-August 2012, a series of morphologic and hydrodynamic observations were undertaken at Bondi Beach (McCarroll et al., 2016), including three days of Lagrangian drifter observations. This study focusses on a single day of drifter deployments on 3/8/12, with a full topo-bathymetric survey of the beach, surfzone and outer-embayment conducted on 6/8/12. The topo-bathymetric survey (Fig 2a) was conducted with a backpack mounted RTK-GPS for the sub-aerial beach, laser-total station for the intertidal and personal watercraft with mounted echosounder and RTK-GPS for the sub-tidal (McCarroll et al., 2016). A fleet of 34 Lagrangian drifters, sampling at 1 Hz, were deployed over a 3 hour period from mid- to low-tide, with a goal of maximising coverage within the surfzone. Detailed drifter specifications and deployment methods are

given in McCarroll et al. (2014). Five pressure transducers (PT) were deployed during drifter observations and were used to quantify wave conditions and for validating the wave transformation model (Section 3.3). One PT was deployed outside the surfzone in 6 m water depth, with four PTs within the surfzone on bars and in rip channels.

Figure 1. Location map (a) and oblique photo taken on the day of observations (b).
Source for (a) is McCarroll et al., (2016)

3.2. Bathymetric three-dimensionality

Alongshore depth standard deviation (σ_z; Feddersen and Guza, 2003) can be used to quantify beach three-dimensionality:

$$\sigma_z(x) = \sqrt{\frac{1}{y_2 - y_1}\int_{y_1}^{y_2}\left(z(x,y) - \overline{z(x)}\right)^2 dy} \qquad (1)$$

Where (x, y) are the cross- and alongshore coordinates, z is depth and the overbar represents the alongshore depth average for a given cross-shore location. However, on a curved embayed beach, the alongshore direction varies along the beach. A shoreline straightening method (e.g. Harley et al., 2008) was considered inappropriate as it would necessitate transforming the drifter data, potentially altering statistical results (Section 3.4). As an alternative, a localised alongshore direction is determined at all points in the surfzone by minimising:

$$\sigma_z(L,\theta) = min\left[\sqrt{\frac{1}{L}\int_{-\frac{L}{2}}^{\frac{L}{2}}\left(z(L,\theta) - \overline{z(L,\theta)}\right)^2 dL}\right] \qquad (2)$$

Where a line of fixed length L is drawn at a range of angles relative to the y-axis ($-\pi/2 < \theta < \pi/2$) through each grid point, with the minima indicating the direction of lowest alongshore variability (short red lines for selected points shown in Fig 2a). The alongshore length must be greater than bar-rip wavelengths (here L = 400 m). The localised depth standard deviation ($\sigma_z[L', \theta]$) is then calculated at this alongshore direction over a shorter alongshore distance (using [2], with L' = 100 m) to capture bathymetric variation at the scale of the local rip cells (Fig 2b). All subsequent references to σ_z refer to this localised value.

3.3 Wave transformation model

The SWAN model was used to transform offshore wave buoy data (located ~15 km north of the site in 90 m water depth) into the nearshore. A single stationary wave state, with default SWAN settings, was run for the period of drifter observations, with H_s=1.6 m, T_p=11 s, θ=0º (shore normal) and directional spreading = 4

($\cos^m(\theta)$ distribution) . Model results (Fig 2b) compared well with PT observations (maximum H_s error ~0.1 m, T_p error <1 s), and also with video observations of surfzone extent (Fig 1b).

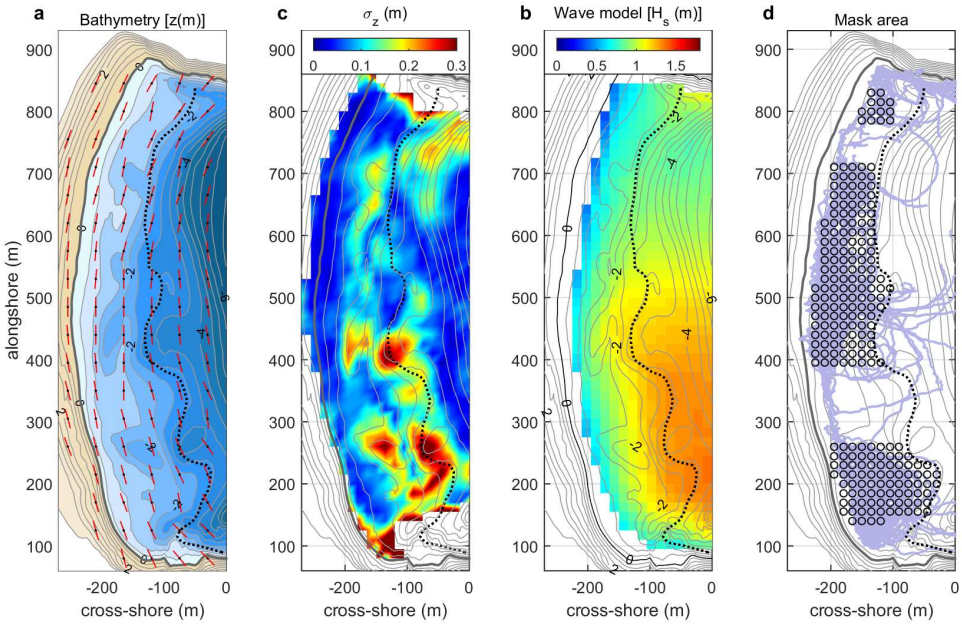

Figure 2. Bondi Beach shoreline is bold (MSL, AHD71), approximate extent of surfzone is dotted, (a) topo-bathymetry, red lines indicate local alongshore direction for selected points (Section 3.2); (b) localised bathymetric standard deviation (Section 3.2); (c) modelled wave height; (d) mask area (circles) used for statistical analysis, overlaid on drifter tracks, headland adjacent areas and zones of low drifter coverage are excluded from analysis.

3.4. Lagrangian velocity and dispersion analysis

All drifter data were low-pass filtered at 0.01 Hz to exclude incident wave oscillations and to minimise infragravity motions related to bound and leaky waves, while capturing the bulk of energy related to vortical surfzone eddy related motions (MacMahan et al., 2004; Feddersen 2014).

Drifter velocities were obtained through position difference over time, with $r_i(t'|\boldsymbol{x})$ the displacement of a drifter at t' seconds after t_0, and subscript-i the cross- or alongshore component. Instantaneous low-pass velocity at time t is $u_i(t|\boldsymbol{x}) = dr_i(t|\boldsymbol{x})/\,dt$, where dt=1 s, the drifter sampling rate. Mean velocities (U_i) were determined for 15 m x 15 m bins ($\boldsymbol{X}$), as ($U_i = \overline{u_i[t \mid \boldsymbol{X}]}$) with overbar representing the time average.

Drifter velocity variability was analysed using a method similar to Spydell et al. (2014), with an anomalous velocity (u_i') determined for each drifter point within bin $\boldsymbol{X}$:

$$u_i'(t|\boldsymbol{X}) = u_i(t|\boldsymbol{X}) - U_i(\boldsymbol{X}) \tag{3}$$

Velocity standard deviation ($\sigma_{U,i}$) is then:

$$\sigma_{U,i}(\boldsymbol{X}) = \sqrt{\frac{1}{n-1}\sum (u_i')^2} \tag{4}$$

Where n is the number of drifter observations (at 1 Hz) in a bin, with $n \geq 100$ required per bin to report a mean velocity and standard deviation. References herein to mean velocity refer to the scalar magnitude

$\left(U = \sqrt{U_i^2 + U_j^2}\right)$ and similarly for velocity standard deviation $\left(\sigma_U = \sqrt{\sigma_i^2 + \sigma_j^2}\right)$, where (*i, j*) are the cross- and alongshore-components.

Dispersion is reported on using the methods of Spydell et al. (2007) and Brown et al. (2009) for single particle diffusivity and dispersion, applicable to an inhomogeneous velocity field. Those methods have been adapted here for spatially-binned values, suitable for assessing flow behaviour on a complex morphology. For a given bin ($\boldsymbol{X}$) over the deployment, a time-series of displacements at 1 Hz is calculated for each drifter entering the bin. Multiple time-series are obtained for a single drifter by incrementing t_0 up to a maximum of t_{150}, with each time-series duration equal to T'= 150 s. Each drifter has 151 displacement time-series' ($t_{0\rightarrow 150\ s}, t_{1\rightarrow 151\ s}, \ldots, t_{150\rightarrow 300\ s}$), each with displacements of $s_i(t' = 1, 2, \ldots, 150 \mid \boldsymbol{X})$. Using this method, drifter runs must be a minimum of 300 s duration after entering the bin. Dispersion and diffusivity statistics ideally require longer time-series, but are limited here by drifter deployment durations and coverage. Drifters may exit or re-enter the cell within the time limit. By averaging over all drifters entering a bin, a mean displacement $S_i(t'|\boldsymbol{X})$ and mean velocity $V_i(t'|\boldsymbol{X})$ are calculated, noting that V is time-dependent and may include points outside the bin, distinguishing it from U.

Anomalous Lagrangian velocities are calculated as the difference between each individual drifter velocity and the time-varying mean:

$$v_i'(\boldsymbol{X}) = v_i(t'|\boldsymbol{X}) - V_i(t'|\boldsymbol{X}) \tag{5}$$

This is used to determine the anomalous Lagrangian velocity auto-covariance, in the cross- (C_{xx}) and alongshore (C_{yy}):

$$C_{ii}(t', \boldsymbol{X}) = \langle v_i'(t'|\boldsymbol{X})\, v_i'(0|\boldsymbol{X})\rangle \tag{6}$$

Angled brackets indicate averaging over all drifters in a bin. Absolute diffusivity, which is the spreading rate, is the integral of the auto-covariance:

$$\kappa_{ii}(t', \boldsymbol{X}) = \int_0^{T'} C_{ii}(t'|\boldsymbol{X})dt' \tag{7}$$

Where T'=150 s. Finally, the displacement variance (or absolute dispersion, D_{ii}^2) is:

$$D_{ii}^2(t', \boldsymbol{X}) = 2\int_0^{T'} \kappa_{ii}(t'|\boldsymbol{X})dt' \tag{8}$$

D_{xx}^2 and D_{yy}^2 are the cross- and alongshore variance in particle displacement, with the standard deviations D_{xx} and D_{yy} indicating the *x*- and *y*-length scales of the patch. The ensemble averaged patch area (m^2) is $\left(D^2 = D_{xx}\, D_{yy}\right)$. The patch length scale (D [m]) is reported on for easy comparison to Brown et al., (2009), representing the average side-length of the patch.

3.5. Forcing control analysis

Areas to be included in statistical analyses are indicated in Figure 2d, excluded are areas outside the surfzone and areas of poor drifter coverage (around *y*=300 m and *y*=750 m). Additionally, headland adjacent areas are excluded as boundary zones experience different forcing controls to the open beach (McCarroll et al., 2014; Castelle et al., 2016), placing them beyond the scope of the hypotheses being tested here.

Linear regression analyses were performed between forcing controls (H_b, σ_z) and surfzone current variables (U, σ_U and D at 120 s). It is noted that waves, currents and bathymetry all mutually interact in a

morphodynamic beach system, such that none are truly independent. However, for the time scales examined here (minutes to hours), it is convenient to examine H_b and σ_z as forcing controls.

In order to directly compare variables, a single value was determined for each variable for each alongshore position. Breaking wave height as a function of alongshore position ($H_b[y]$) was taken as the maximum value of H_s in -200 m < x < 20 m (Fig 2c) for each value of y. Other variables were averaged over the cross-shore for each alongshore position, excluding values outside the masked area (Fig 2d).

4. Results

4.1. Environmental conditions

During the 3 hour period of drifter observations, breaking wave heights were observed and modelled (Fig 2c) to peak at H_b=1.4 m at the southern bar (y=200 m), decreasing to 0.8 m off the northern bar (y=800 m). Peak period was ~11 s across the embayment. Offshore wave direction was near shore-normal, with waves refracting to shore normal at the breakpoint along the curved embayment. The surfzone width and active area of surfzone currents (Fig 2d) was 150 m at the southern bar, decreasing to 70 m at the northern bar. Water levels decreased from mid- to low-tide, over a range of 0.6 m. Winds were slight and offshore.

4.2 Beach state and morphology

The southern half of the beach exhibited a complex multi-bar beach state (Fig 2b,c), with an inner transverse-bar-and-rip (TBR; Wright and Short, 1984) as well as an outer TBR. The outer bar-rip system was formed during storm conditions (McCarroll et al., 2016), and was mostly inactive under the moderate wave forcing at the time of observations (Fig 2a). The northern end of the beach was in the modal lower-energy state of a single-bar, low-tide-terrace.

Although the beach was highly three-dimensional (Fig 2b), recent storms had flattened the lower beachface and inner surfzone, such that bar-rip morphology occurred mostly below the z=-1 m contour. The major rip channels of the active inner-bar system (headland rips excluded) were at y=250 m, 450 m and 700 m, with peak σ_z of 0.3 m, 0.25 m and 0.18 m respectively (Fig 2b). This supports the commonly observed, but rarely quantified hypothesis that bathymetric three-dimensionality increases with alongshore wave height.

4.3. Mean and variable flow velocity

A summary of mean and variable Lagrangian velocities is displayed in Figure 3. Initial inspection of instantaneous velocities (Fig 3a) indicates a generally decreasing trend from the high-energy southern end to low-energy northern end, though this trend is less apparent in the mean velocity field (Fig 3b). Peak instantaneous (>1 m s^{-1}) and mean velocities (>0.5 m s^{-1}) occur in the outer part of the rip-cell circulation at y=200 m, while mean velocities associated with the oblique rip cell at y=450 m are relatively low. A region of anomalously high (0.4 m s^{-1}) southward alongshore-meandering mean flow is present at y=600 m.

Velocity standard deviation (σ_U), a measure of low frequency variability due to vortical forcing, generally increases in the direction of increasing wave height (north to south), with peak values of >0.4 m s^{-1} over the southern bar (y=200 m), decreasing to <0.2 ms^{-1} over the northern bar (y=800 m). By contrast, σ_U does not appear to be clearly correlated with areas of high bathymetric variability, for example in the southern rip channel (y=250 m) σ_U is only 0.2 m s^{-1}, while in the mid-beach oblique rip channel at y=450 m, σ_U is a relatively high 0.35 m s^{-1}.

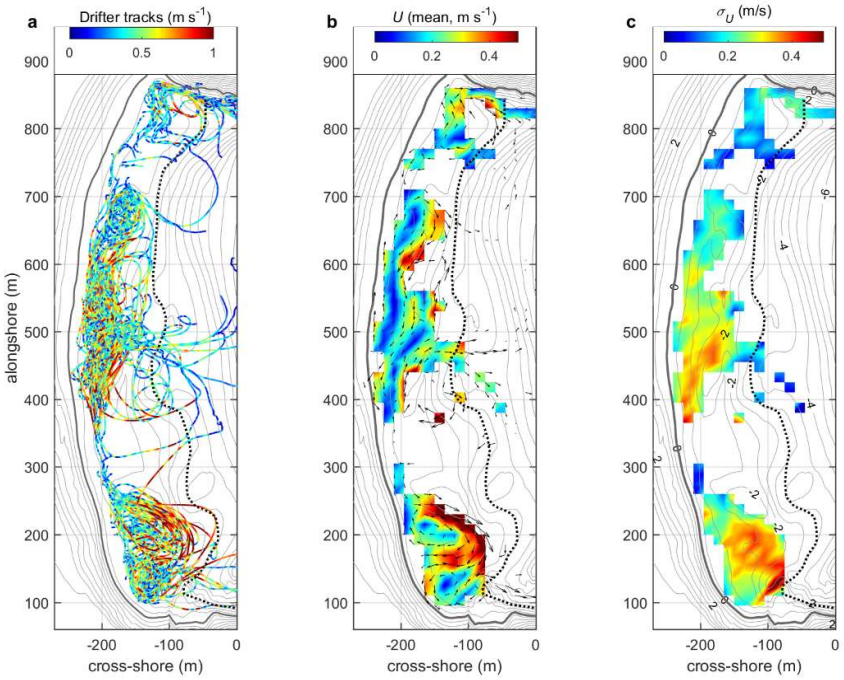

Figure 3. Lagrangian velocity, (a) drifter tracks with colour indicating instantaneous low-pass velocity [u]; (b) 15 x 15 m binned mean velocity [U]; and (c) binned velocity standard deviation [σ_U].

4.4. Surfzone dispersion and diffusivity

A synoptic time-series of surfzone dispersion is shown in Figure 4, values represent the time-averaged cross- and alongshore length scale that an arbitrarily small patch of water, originating in a given grid cell, would spread to after the time interval indicated. This statistic does not describe how far that patch would travel from the grid cell of origin, which is instead described by mean velocity (Fig 3).

Total dispersion length scales varied from 10-50 m after 150 s (Fig 4), with maximum values near the middle of the beach, peaking around y=510 m. Interestingly, the southern zone (Block 1), which experienced the highest waves (Fig 2c), the greatest depth alongshore standard deviation (σ_z, Fig 2b), as well as the highest velocities (U and σ_U; Fig 3), is not the most dispersive zone over this time-frame. Block 1 dispersion values are highly variable, with high values in the outer rip flow at y=220 m and over the narrow bar at y=160 m (D>50 m), interspersed with lower values. Block 2 appears to be more consistently dispersive with the bulk of values from 30-50 m. There is no obvious cross-shore distribution pattern, although dispersion does appear to decrease from the middle to the northern end of the beach.

Absolute diffusivity, the rate of dispersion, is examined in in Figure 5. The length of the beach was divided into four sections (Block 1-4, Fig 4a), in order to compare alongshore variations, with time-series' for the cross- (κ_{xx}) and alongshore (κ_{yy}) components of diffusivity for each block. The full range of grid cell diffusivity values are broadly overlapping (grey lines in Fig 5), however there are substantial differences between directional components as well as in the alongshore that can be identified.

Examining κ_{xx}, the curves for Blocks 1-3 follow a similar shape, with a rapid period of diffusivity increase from 0 to 10 s, that flattens and peaks at ~75 s at 1-1.5 m^2 s^{-1}. This may reflect the dispersive motion of individual waves, smoothed by the 0.01 Hz low pass filter, and may also include rip-current related dispersion for some cells. After ~100 s, diffusivity in Blocks 1-3 gradually decrease, indicating the patch is still spreading in the cross-shore, though at a decreasing rate. Cross-shore diffusivity for Block 4 increases at a

lower rate, possibly reflecting lower wave energy, but does not peak over the short time-series.

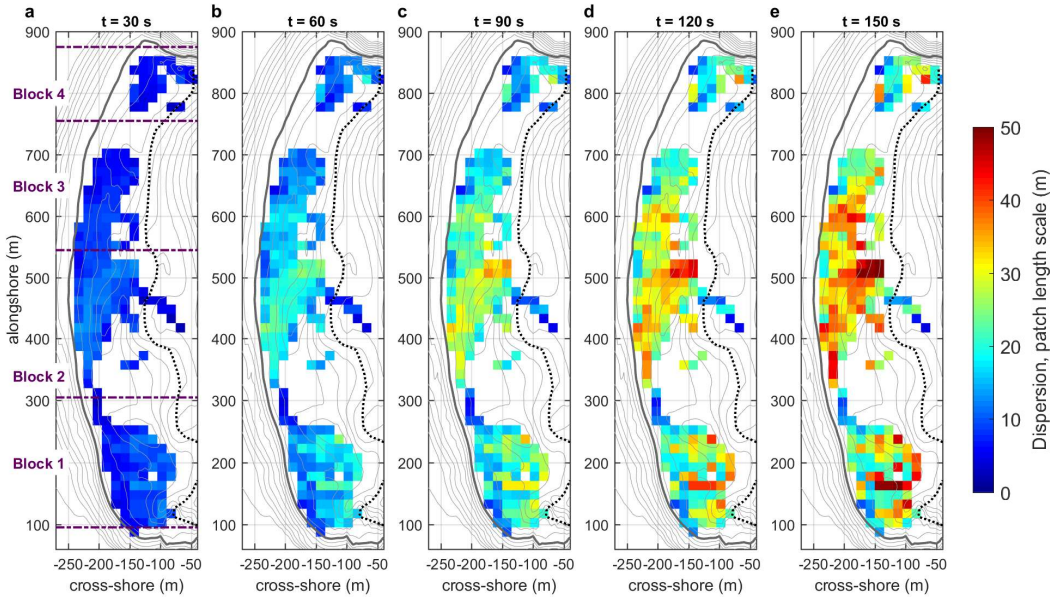

Figure 4. Dispersion synoptic time-series (patch length, *D*[m]), at lags of (a) 30 s; (b) 60 s; (c) 90 s; (d) 120 s; and (e) 150 s. Blocks 1-4 used in Figure 5 are indicated in (a).

Alongshore diffusivity rates (κ_{yy}) initially increase more slowly than in the cross-shore. However, κ_{yy} tends to peak at higher values ($\kappa_{yy} = 3.8\ \mathrm{m^2 s^{-1}}$ at 90 s, Block 2) and continues to increase for a longer duration (e.g. Block 3). These data suggest that cross-shore diffusivity is broadly similar across Blocks 1-3 and that the main factor in differentiating dispersion rates in the alongshore is κ_{yy}. Block 1 κ_{yy} is skewed positive, with a small number of high values increasing the average. The low energy zone (Block 4) is less dispersive in the alongshore than other parts of the beach.

Dispersion is summarised in Figure 6, values represent the mean length along each axes of a patch, so a length of $D = 10$ m, is equivalent to a patch area of $D^2 = 100\ \mathrm{m^2}$. Curves for all alongshore blocks (Fig 6) follow a decreasing trajectory, with dispersion length scales of 20-35 m after 150 ss. As suggested by the synoptic dispersion (Fig 4) and diffusivity data (Fig 5), absolute dispersion over this time-frame is greatest in Block 2 (*D*=35 m after 150 s), near the middle of the beach. Block 1 and 3 are similar in magnitude, with the lowest rates of dispersion at the northern end of the beach. These observations are inconsistent with the hypotheses that rates of dispersion will increase with (i) wave height; and (ii) beach three-dimensionality, as both of these forcing factors peak at the southern end, not the middle of the beach.

4.5. Forcing relationships

The forcing (H_b, σ_z) and current variables (U , σ_U and D at 120 s) are represented in Figure 7 as a function of alongshore position. Breaking wave height (SWAN model output) peaks at 1.4 m at *y*=200 m (Fig 7a), then decreases steadily to the north (increasing *y*), to reach a minima of 0.8 m at *y*=780. Alongshore depth standard deviation (Fig 7b) within the masked area (Fig 2d) is higher at the southern end, with both the mean values of σ_U and cross-shore variability (error bars in Fig 7b), decreasing north of y=450 m.

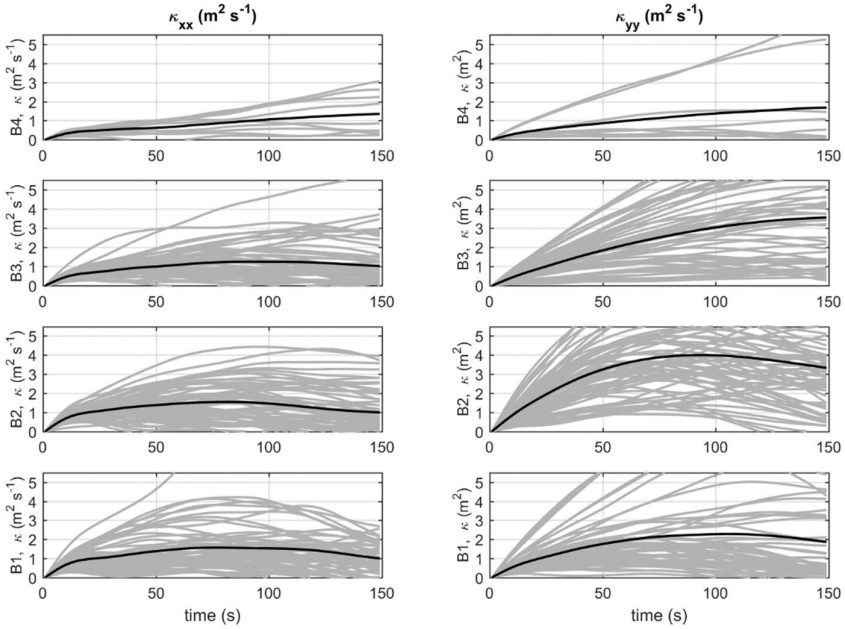

Figure 5: Time-series of cross-shore (κ_{xx}) and alongshore (κ_{yy}) diffusivity (spreading rate). B1-B4 are Blocks 1 (so uth) to Block 4 (north) indicated in Fig 4a. Mean curves (black lines) and individual grid cells (grey lines) indicated. M ask (Fig 2d) applied to exclude headland areas, low drifter coverage areas and areas outside the surfzone.

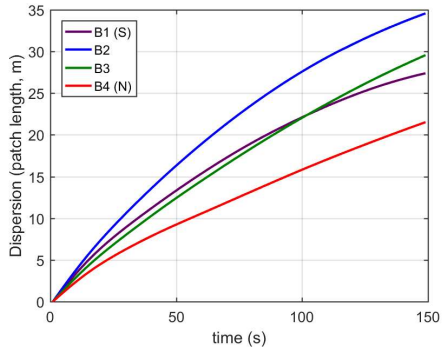

Figure 6. Dispersion magnitude (patch length scale) mean time-series for each of the Blocks 1-4, indicated in Fig 4a. Areas outside the mask in Figure 2d are excluded from this calculation.

Current velocity (Fig 7c-d) values generally decrease towards the north, though with some anomalous zones. For example, mean velocity (Fig 7c) spikes at y=620 m, seemingly uncorrelated with waves or bathymetry. Given that wave angle is shore-normal, strong alongshore currents in this area may be related to the alongshore wave height gradient and the transition from multi- to single-bar (Fig 2). Variable velocity (Fig 7d) has the clearest visual correlation with alongshore wave height. Consistent with the analysis in Section 4.2, dispersion increases slightly from the south end to the middle of the beach (Fig 7e), then decreases towards the northern end.

Linear regression statistics between the variables in Figure 7 are presented in Table 1. Breaking wave height was found to be significantly correlated with bathymetric variability, mean current velocity and current standard deviation. Each of these relationships has a high degree of scatter (low R^2), but is robust ($p<0.002$). The strongest correlation is between wave height and flow variability (R^2=0.50; p=2 x 10^{-6}). Alongshore depth standard deviation was found to be weakly correlated with mean velocity (R^2=0.21; p=0.01).

Dispersion was not significantly correlated with either H_b or σ_z.

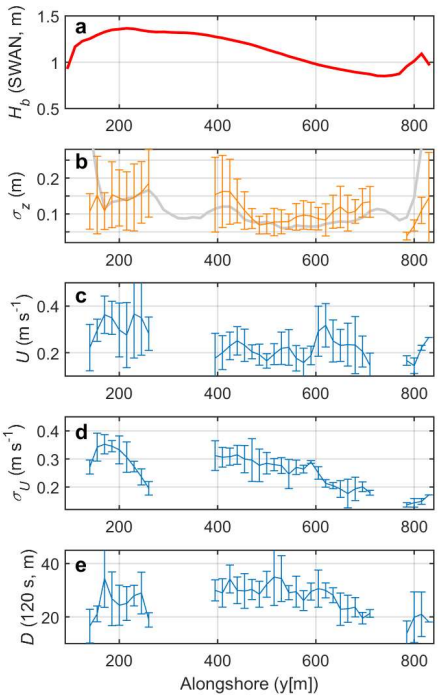

Figure 7. Alongshore values for hydrodynamic and bathymetric variables, (a) breaking wave height [H_b]; (b) alongshore depth standard deviation [σ_z]; (c) mean velocity [U]; (d) velocity standard deviation [σ_U]; and (e) dispersion length scale [D] at 120 s. Panels (b-e) are cross-shore averages of the grid cell mean values (e.g. see Fig 3b for U), for each alongshore position, with error bars indicating one standard deviation. Values outside the mask area (Fig 2d) are excluded. Grey line in (b) represents the full beach extent (not masked) for σ_z.

Table 1. Wave forcing, bathymetry and surfzone current linear relationships.

Variable 1	Variable 2	R^2	p
H_b	σ_z	**0.28**	**0.001**
	U	**0.26**	**0.002**
	σ_U	**0.50**	**0.000**
	D	0.06	0.16
σ_z	U	**0.21**	**0.01**
	σ_U	0.08	0.11
	D	0.01	0.61

Significant relationships are bold and shaded. σ_z –alongshore depth standard deviation; U – mean velocity; σ_U –low-pass velocity standard deviation; D – dispersion patch length scale after 120 s.

5. Discussion

This study is a proof of concept for a method to test forcing controls on surfzone currents. Given the single day of observations used, only preliminary conclusions can be drawn from the linear correlations in Table 1. The force-response relationships that have previously been established are confirmed by this study and are generalised to the entire surfzone, suggesting this method warrants further application.

A shortcoming of the approach taken here is that no attempt has been made to normalise (non-

dimensionalise) the linear relationships (e.g. by Froude number or dimensionless depth; MacMahan et al., 2006). Therefore, it becomes difficult to distinguish between wave height and bathymetric variability as forcing controls when those variables are themselves correlated. This, in addition to the limited sample and complex bathymetry, may be responsible for the low coefficients of determination in Table 1. Additionally, there are a number of key variables that were not tested, including: directional spreading of the wave field, water level, current directional standard deviation and vorticity. These issues can be addressed in a future effort.

Wave height forcing relationships were well supported. First, the relationship between breaking wave height and bathymetric three-dimensionality is confirmed. While this relationship is well-known and has been shown previously (e.g. Ranasinghe et al., 2004), the novel method presented here is flexible and does not require a coordinate transformation. Second, the surfzone-wide correlation between breaking wave height and mean flow velocity expands upon previous efforts that focus upon mean velocity in the rip channel (e.g. MacMahan et al., 2006). This result is expected, as it follows that if rip channel mean velocity scales with wave height, there should also be an increase in mean flow in other parts of the rip-cell (bar, feeder and outer-circulation). Third, the relationship between alongshore H_b and σ_U was found to be robust, supporting MacMahan et al. (2004) who tested the same relationship through H_b variations over time.

Bathymetric forcing relationships were found to be weak or not present. The known-relationship between σ_z and U was confirmed, though with a much weaker correlation than previous efforts (e.g. Castelle et al., 2010; McCarroll et al., 2014). This may be related to the complex bathymetry on the observed beach, the anomalously high alongshore velocities (Fig 7c) and the lack of normalisation in the statistical analysis. Bathymetric variability was found to be uncorrelated with velocity variability, inconsistent with the hypothesis of Castelle et al. (2010) that deeper rip channels exhibit greater velocity pulsing. The evidence on this relationship is scant and further investigation is required.

Dispersion was found to be uncorrelated with both H_b and σ_z. Previous results (Spydell et al., 2007; Brown et al., 2009) suggest that dispersion may increase with wave height, however this relationship has not been clearly determined and further effort is required. It may be that surfzone exit rates and rip channel orientation (Figs 3,4), have a greater impact than wave height and channel depth. Given that exit rates are hypothesised to decrease with wave height (Castelle et al., 2014), there may be a non-linear relationship between wave height and dispersion. In general, observed rates of dispersion were of similar magnitude to Brown et al. (2009), including κ_{xx} initially being greater, before being overtaken by κ_{yy}.

6. Conclusion

A novel method for determining forcing relationships across the surfzone of embayed beaches was presented. Statistically significant positive relationships were demonstrated between breaking wave height and bathymetric variability, mean velocity and velocity standard deviation. Bathymetric variability was found to be correlated with mean velocity, but not velocity standard deviation. This study is the first attempt to examine the spatial distribution of 3D-surfzone dispersion, finding that rates of dispersion were uncorrelated with wave height and bathymetry. Given further development and additional data, these methods represent a promising approach to investigate many of the unclear scaling relationships between wave forcing, bathymetry and surfzone currents on three-dimensional beaches.

Acknowledgements

Field observations were funded by Australian Research Council (ARC) Linkage Project LP110200134 and Surf Life Saving Australia. Many thanks to Ben Van Leeuwen, Ian Turner, Hannah Power, Mark Davidson, all fieldwork volunteers, Waverly council lifeguards and the Australian Lifeguard Service. Sydney wave buoy data were provided by Manly Hydraulics Lab on behalf of the NSW Office of Environment and Heritage.

References

Bowen, A.J., 1969. Rip currents: 1. Theoretical investigations. *Journal of Geophysical Research,* 74(23): 5467-5478.

Brown, J., MacMahan, J., Reniers, A. and Thornton, E., 2009. Surf zone diffusivity on a rip-channeled beach. *Journal of Geophysical Research: Oceans,* 114(C11): C11015.

Castelle, B., Michallet, H., Marieu, V., Leckler, F., Dubardier, B., Lambert, A. and Bouchette, F., 2010. Laboratory experiment on rip current circulations over a moveable bed: Drifter measurements. *Journal of Geophysical Research: Oceans*, *115*(C12).

Castelle, B. and Coco, G., 2012. The morphodynamics of rip channels on embayed beaches. *Continental Shelf Research,* 43: 10-23.

Castelle, B. and Coco, G., 2013. Surf zone flushing on embayed beaches. *Geophysical Research Letters,* 40(10): 2206-2210.

Castelle, B., Reniers, A. and MacMahan, J., 2014. Bathymetric control of surf zone retention on a rip-channelled beach. *Ocean Dynamics,* 64(8): 1221-1231.

Castelle, B., Scott, T., Brander, R. and McCarroll, R., 2016. Rip current types, circulation and hazard. *Earth-Science Reviews,* 163: 1-21.

Feddersen, F., 2014. The Generation of Surfzone Eddies in a Strong Alongshore Current. *Journal of Physical Oceanography,* 44(2): 600-617.

Feddersen, F. and Guza, R., 2003. Observations of nearshore circulation: Alongshore uniformity. *Journal of Geophysical Research,* 108(C1): doi: 10.1029/2001JC001293.

Harley, M.D. and Turner, I.L., 2008. A simple data transformation technique for pre-processing survey data at embayed beaches. *Coastal Engineering,* 55(1): 63-68.

Hsu, J.R., Yu, M., Lee, F. and Benedet, L., 2010. Static bay beach concept for scientists and engineers: a review. *Coastal Engineering,* 57(2): 76-91.

Johnson, D. and Pattiaratchi, C., 2006. Boussinesq modelling of transient rip currents. *Coastal Engineering,* 53(5): 419-439.

MacMahan, J., Brown, J., Brown, J., Thornton, E., Reniers, A., Stanton, T., Henriquez, M., Gallagher, E., Morrison, J., Austin, M.J., Scott, T.M. and Senechal, N., 2010. Mean Lagrangian flow behavior on an open coast rip-channeled beach: A new perspective. *Marine Geology,* 268(1): 1-15.

MacMahan, J.H., Reniers, A.J., Thornton, E.B. and Stanton, T.P., 2004. Surf zone eddies coupled with rip current morphology. *Journal of Geophysical Research,* 109(C7): doi:10.1029/2003JC002083.

MacMahan, J.H., Thornton, E.B. and Reniers, A.J., 2006. Rip current review. *Coastal Engineering,* 53(2): 191-208.

McCarroll, R.J., Brander, R.W., Turner, I.L., Power, H.E. and Mortlock, T.R., 2014. Lagrangian observations of circulation on an embayed beach with headland rip currents. *Marine Geology,* 355: 173-188.

McCarroll, R.J., Brander, R.W., Turner, I.L. and Van Leeuwen, B., 2016. Shoreface storm morphodynamics and mega-rip evolution at an embayed beach: Bondi Beach, NSW, Australia. *Continental Shelf Research,* 116: 74-88.

Peregrine, D., 1999. Large-scale vorticity generation by breakers in shallow and deep water. *European Journal of Mechanics-B/Fluids,* 18(3): 403-408.

Ranasinghe, R., Symonds, G., Black, K. and Holman, R., 2004. Morphodynamics of intermediate beaches: a video imaging and numerical modelling study. *Coastal Engineering*, *51*(7), 629-655.

Reniers, A. J. H. M., MacMahan, J. H., Thornton, E. B. and Stanton, T. P., 2007. Modeling of very low frequency motions during RIPEX. *Journal of Geophysical Research: Oceans*, *112*(C7).

Reniers, A.J., MacMahan, J., Thornton, E., Stanton, T., Henriquez, M., Brown, J., Brown, J. and Gallagher, E., 2009. Surf zone surface retention on a rip□channeled beach. *Journal of Geophysical Research,* 114(C10): doi:10.1029/2008JC005153.

Short, A.D., 1999. *Handbook of Beach and Shoreface Morphodynamics*, John Wiley & Sons, Chichester.

Short, A.D. and Trenaman, N., 1992. Wave climate of the Sydney region, an energetic and highly variable ocean wave regime. *Marine and Freshwater Research,* 43(4): 765-791.

Silva, R., Baquerizo, A., Losada, M.Á. and Mendoza, E., 2010. Hydrodynamics of a headland-bay beach—Nearshore current circulation. *Coastal Engineering,* 57(2): 160-175.

Spydell, M., Feddersen, F., Guza, R.T. and Schmidt, W.E., 2007. Observing Surf-Zone Dispersion with Drifters. *Journal of Physical Oceanography,* 37(12): 2920-2939.

Spydell, M.S., Feddersen, F., Guza, R. and MacMahan, J., 2014. Relating Lagrangian and Eulerian horizontal eddy statistics in the surfzone, *Journal of Geophysical Research: Oceans*, 119(2): 1022-1037.

Suanda, S.H. and Feddersen, F., 2015. A self□similar scaling for cross□shelf exchange driven by transient rip currents. *Geophysical Research Letters,* 42(13): 5427-5434.

Wright, L.D. and Short, A.D., 1984. Morphodynamic variability of surf zones and beaches: A synthesis. *Marine Geology,* 56: 93-118.